37. S. F. Singer, *EOS* **80**, 183 (1999); P. J. Michaels, *World Clim. Rep.* **4**(17), 1 (1999); testimony before the Committee on Government Reform, Subcommittee on National Economic Growth, Natural Resources and Regulatory Affairs, and Committee on Science, Subcommittee on Energy and Environment, U.S. House of Representatives, joint hearing on "Is CO_2 a Pollutant and Does EPA Have the Power to Regulate It?", Washington, DC, 6 October 1999.
38. J. R. Christy and R. T. McNider, *Nature* **367**, 325 (1994); P. D. Jones, *Geophys. Res. Lett.* **21**, 1149 (1994); S. F. B. Tett, J. F. B. Mitchell, D. E. Parker, M. R. Allen, *Science* **274**, 1170 (1996).
39. See Web table 2 at *Science* Online (www.sciencemag.org/feature/data/1046025.shl).
40. Bengtsson *et al.* (*12*), in their analysis of various realizations (*34*) of the GSOP experiment, show slight warming (by roughly +0.01° to +0.03°C per decade) of the model surface temperature relative to temperatures at 850 and 500 hPa. These results are not inconsistent with our finding of a slight cooling (by −0.035°C per decade) of the surface relative to lower troposphere in the single GSOP experiment we consider (Fig. 5C). These small differences arise from our use of a vertically weighted lower tropospheric temperature (the 2LT retrieval) rather than discrete temperatures at 850 and 500 hPa, and from our masking procedure, which excludes areas of large surface warming at high latitudes in both hemispheres [see (*12*), plate 3].
41. K. P. Shine, Y. Fouquart, V. Ramaswamy, S. Solomon, J. Srinivasan, in *Climate Change 1995: The Science of Climate Change*, J. T. Houghton *et al.*, Eds. (Cambridge Univ. Press, Cambridge, 1996), pp. 108–131; J. E. Hansen, M. Sato, R. Ruedy, *J. Geophys. Res.* **102**, 6831 (1997); T. K. Berntsen *et al.*, *J. Geophys. Res.* **102**, 28101 (1997).
42. Examples include the effects of El Chichón and other volcanic eruptions [N. G. Andronova, E. V. Rozanov, F. Yang, M. E. Schlesinger, G. L. Stenchikov, *J. Geophys. Res.* **104**, 16807 (1999)], as well as aerosols resulting from biomass burning [J. E. Penner, R. Dickinson, C. O'Neill, *Science* **256**, 1432 (1992)] and mineral dust [I. Tegen and I. Fung, *J. Geophys. Res.* **100**, 18707 (1995)].
43. National Research Council, Board on Atmospheric Sciences and Climate, Commission on Geosciences, Environment and Resources, *Reconciling Observations of Global Temperature Change* (National Academy Press, Washington, DC, 2000).
44. D. J. Gaffen *et al.*, *Science* **287**, 1242 (2000).
45. B. D. Santer *et al.*, *Nature* **384**, 523 (1996); T. M. L. Wigley, P. J. Jaumann, B. D. Santer, K. E. Taylor, *Clim. Dyn.* **14**, 781 (1998); S. F. B. Tett *et al.*, *Nature* **399**, 569 (1999); K. Hasselmann, *J. Clim.* **6**, 1957 (1993).
46. Supported by NOAA Office of Global Programs ("Climate Change Data and Detection") grant NA87GP0105 (T.M.L.W.) and U.S. Department of Energy (DOE) grant DE-FG02-98ER62601 (P.D.J. and T.M.L.W.). Work at Lawrence Livermore National Laboratory was performed under the auspices of the Environmental Sciences Division of DOE (contract W-7405-ENG-48). We thank J. R. Christy for the MSU data and static MSU weighting functions, and C. F. Keller, G. C. Hegerl, J. M. Wallace, M. C. MacCracken, A. Robock, and two anonymous reviewers for useful comments and suggestions that substantially improved the manuscript.

5 October 1999; accepted 29 December 1999

Crystal Structure of the Ribonucleoprotein Core of the Signal Recognition Particle

Robert T. Batey,[1] Robert P. Rambo,[1] Louise Lucast,[2] Brian Rha,[2] Jennifer A. Doudna[2*]

The signal recognition particle (SRP), a protein-RNA complex conserved in all three kingdoms of life, recognizes and transports specific proteins to cellular membranes for insertion or secretion. We describe here the 1.8 angstrom crystal structure of the universal core of the SRP, revealing protein recognition of a distorted RNA minor groove. Nucleotide analog interference mapping demonstrates the biological importance of observed interactions, and genetic results show that this core is functional in vivo. The structure explains why the conserved residues in the protein and RNA are required for SRP assembly and defines a signal sequence recognition surface composed of both protein and RNA.

Cells communicate with their surroundings by means of proteins that either reside within cellular membranes or are secreted to the outside. One of the principal pathways for targeting these proteins uses the SRP to catalyze cotranslational transport of nascent secretory and membrane proteins to the endoplasmic reticulum (ER) in eukaryotes and to the plasma membrane in prokaryotes. The well-characterized eukaryotic SRP, an evolutionarily conserved ribonucleoprotein complex, recognizes the NH_2-terminal signal sequence of targeted proteins as they emerge from the ribosome. Binding to the SRP arrests polypeptide elongation and mediates docking of the translating ribosome with receptors on the ER in a guanosine 5′-triphosphate (GTP)–dependent process (Fig. 1A) (*1*, *2*).

In bacteria, the SRP is essential for cell viability and efficient protein export (*3*) and consists of the 4.5*S* RNA and the Ffh protein. These components as well as the SRP receptor, FtsY, share sequence and functional homology with their eukaryotic counterparts 7SL RNA, SRP54, and SRα, respectively (*4*–*8*). The evolutionary conservation of this fundamental cellular component is demonstrated by the ability of human SRP54 to bind with high affinity to the *Escherichia coli* 4.5*S* RNA and to rapidly hydrolyze GTP in the presence of the SRP receptor (*5*). Similarly, Ffh is able to replace SRP54 in a chimeric mammalian SRP that is capable of elongation arrest and signal sequence recognition (*6*). Thus, the Ffh-4.5*S* RNA complex appears to be a minimized structural and functional homolog of the eukaryotic SRP, which makes it attractive for detailed structural and mechanistic studies.

The Ffh/SRP54 proteins contain three domains: N, G, and M. The NH_2-terminal N domain, a four-helix bundle, is closely associated with the adjacent G domain, a Ras-like guanosine triphosphatase (GTPase) (*9*) responsible for mediating the interaction of the SRP with its receptor and regulating SRP function through hydrolysis of GTP (*7*, *10*). Structurally related N and G domains are also present in the SRP receptor (*11*). The methionine-rich M domain near the COOH-terminus of Ffh/SRP54 contains recognition sites for both the signal peptide and the SRP RNA (*12*–*14*).

The Ffh binding site on the 4.5*S* RNA is localized to domain IV, a ~50-nucleotide (nt) region whose highly conserved secondary structure consists of two internal loops that include noncanonical base pairings and unpaired nucleotides (Fig. 1, B and C) (*15*–*18*). In bacterial and human SRP, several lines of evidence suggest that domain IV (Fig. 1, B and C) stabilizes the particle and its interaction with the signal peptide (*19*, *20*). Outside of domain IV, the size, sequence, and secondary structure of SRP RNAs vary widely, even among bacterial species (*21*), and it is unclear if these regions of the RNA are essential for SRP function.

Here we present the 1.8 Å resolution crystal structure of the universally conserved ribonucleoprotein core of the SRP, a complex between domain IV of 4.5*S* RNA and the M domain of Ffh. Nucleotide analog interference mapping and genetic results show that the structure represents the functional complex in vivo. In the structure, unique RNA-protein interactions characterize the molecular interface, and a network of highly ordered waters and metal ions also mediate key contacts. The structure explains why phylogenetically conserved residues in the protein and RNA are required for SRP assembly, and it suggests a possible role for the RNA in molecular recognition of signal peptides.

Structure determination and overview. To obtain well-ordered crystals of the M domain in complex with SRP RNA, we

[1]Department of Molecular Biophysics and Biochemistry, [2]Howard Hughes Medical Institute, Yale University, New Haven, CT 06511, USA.

*To whom correspondence should be addressed. E-mail: doudna@csb.yale.edu

screened a series of modified protein and RNA constructs (*22*). None of these modifications altered the apparent dissociation constant of the RNA-protein complex from that of the intact *E. coli* SRP, which is 40 pM under the assay conditions we used (*23*). Crystals of the M domain bound to a 49-nt SRP RNA were grown that diffract x-rays to 1.55 Å resolution. The structure was solved by multiwavelength anomalous dispersion (MAD) phasing from crystals containing selenomethionine-labeled protein (Table 1). Using diffraction data extending from 30.0 to 1.8 Å resolution, a model of the complex was built and refined to a crystallographic *R* factor of 19.9% and a free *R* factor of 22.1% (Table 1).

The structure reveals minor groove recognition of a noncanonical RNA helix by a helix-turn-helix (HTH) motif contained within the five α helices of the M domain (Fig. 2, A and B). The HTH fold, corresponding to helices 2 to 4 (Figs. 1D and 2A), is virtually identical to that observed in the crystal structure of the Ffh protein alone as well as that of the M domain of the human SRP54 protein (*24–26*) (Fig. 2A). The HTH motif presents two α helices to the minor groove of the RNA, making a series of direct and solvent-mediated contacts between conserved amino acids and nucleotides. This mode of binding is distinct from that observed for the structurally similar HTH motifs of DNA binding proteins, which bind to DNA primarily through interactions of a single helix in the major groove (*27*). A 33–amino acid segment of the protein containing the proposed signal peptide recognition site is disordered in the crystals and was not observed in the electron density map (Figs. 1D and 2A). This observation is consistent with biochemical evidence for conformational flexibility of this region in the absence of a bound signal sequence (*20*).

In contrast to the protein, the structure of the RNA changes significantly upon binding to the M domain (Fig. 2C). Solution nuclear magnetic resonance (NMR) structures of domain IV of the RNA showed the nucleotide bases of both internal loops stacked into the helix (*16–18*). In the complex, however, the four nucleotides of the asymmetric loop of the RNA are extruded from the helix. Three of these bases are stacked and wrap around the outside of the helix to form a unique surface that positions invariant nt A39 for contacts with the M domain.

Minor groove recognition mediated by two RNA internal loops. The internal loop nucleotides in domain IV of the 4.5*S* RNA create an unusual surface along the minor groove face of the helix that forms the recognition site for the M domain of Ffh. The

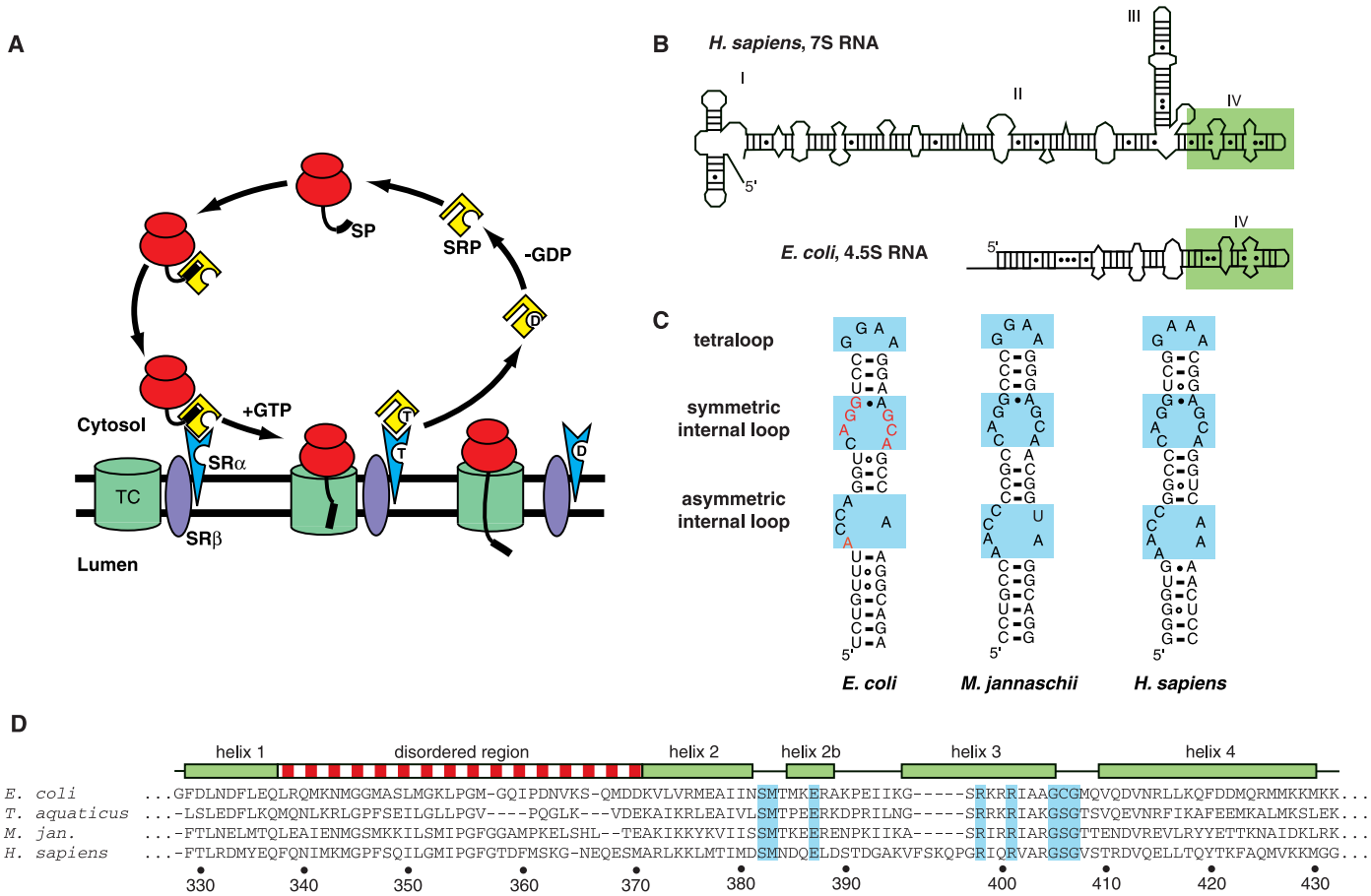

Fig. 1. (**A**) The protein translocation cycle catalyzed by the eukaryotic SRP. A nascent polypeptide chain attached to the ribosome (red) contains a signal sequence (SP) that is recognized by the SRP (yellow), targeting the complex to the translocon (TC) embedded in the ER membrane in a GTP-dependent process [adapted from (*40*)]. (**B**) Schematic of the secondary structure of the SRP RNA from humans and *E. coli*. The universally conserved domain IV of the RNA is highlighted in green. (**C**) Nucleotide sequences of SRP RNA domain IV from representative organisms of the three kingdoms of life. The three principal conserved features of this domain, the GNRA tetraloop, the symmetric internal loop, and the asymmetric internal loop, are highlighted in cyan. Nucleotides in red in the *E. coli* SRP domain IV RNA are those that have been shown to be important for in vivo function (*35*) as well as Ffh binding (*15*). (**D**) Sequence alignment of SRP54/Ffh M domains from various organisms, with the numbering consistent with that of *E. coli* Ffh. The secondary structural assignments were based on the x-ray structure of the bound *E. coli* M domain. Boxed in cyan are invariant residues in the RNA binding region of the protein. The sequence of the *E. coli* M domain shown corresponds to the one that was used for crystallization. Single-letter abbreviations for the amino acid residues are as follows: A, Ala; C, Cys; D, Asp; E, Glu; F, Phe; G, Gly; H, His; I, Ile; K, Lys; L, Leu; M, Met; N, Asn; P, Pro; Q, Gln; R, Arg; S, Ser; T, Thr; V, Val; W, Trp; and Y, Tyr.

nucleotides of the symmetric internal loop of the RNA form five noncanonical base pairs that fill the minor groove and create a unique surface recognized by the protein (Fig. 3A). A symmetric heteropurine G-A base pair is adjacent to a sheared G-G pair that pinches together the opposing strands of the RNA backbone. The narrowed helical cross section is maintained by two structurally distinct A-C base pairs, stacked beneath the G-G pair. Although the Watson-Crick face of the C in each case interacts with the Hoogsteen face of the A, the A47-C62 pair involves two hydrogen bonds between the bases, while the bases in the C46-A63 pair are bridged in part by a potassium ion (Fig. 3A). The phosphodiester backbone in this region interacts directly with the bases of G61, A63, and C46, stabilizing the unusual base pairs. A cross-strand stack between G61 and C46 displaces the A47-C62 base pair from the helical axis (Fig. 3A). Consequently, the A47-C62 pair is thrust into the minor groove, presenting the carbonyl and exocyclic amine groups of C62 and A47, respectively, for direct recognition by the M domain. As a result of the unique set of base pairs in the symmetric loop, the minor groove surface is flat compared with that of a normal A-form helix and contains a binding pocket for a second potassium ion situated at the G-G pair (Fig. 3B). Notably, there is a dense network of hydrogen bonds between the protein and the RNA in this region (Fig. 3A), most of which involve backbone carbonyl groups in the protein rather than specific side chains. This differs from most protein–nucleic acid complexes in which groove interactions are mediated by protein side chains (*28*, *29*).

In the asymmetric internal loop of the RNA, the single unpaired adenosine on the 3′ side remains stacked in the helix. The phosphodiester backbone of the four nucleotides on the 5′ side of the loop is inverted such that the phosphates are pointed toward the interior of the helix. The nucleotide bases are completely expelled from the helix, and nt A39, C40, and C41 stack perpendicular to the helical axis to form an arch that crosses the major groove (Figs. 2A and 3B). A42, a nonconserved residue, is unstacked and serves as a connector between the stack and the helix above it. This unique geometry positions the universally conserved nt A39 to contact invariant residues in both the symmetric internal loop of the RNA and in the protein (Figs. 2A and 3B).

The heart of the RNA-protein interface is a protein-mediated interaction between the symmetric and asymmetric internal loops. A dense network of contacts occurs between helices 2b and 3 in the M domain (Fig. 1D) and the A47-C62 pair and A39 in the RNA (Fig. 4A). The location of A39 on the outside of the RNA helix enables stacking with the first invariant arginine residue (Arg-398) and hydrogen bonding to the second (Arg-401) within the highly conserved amino acid sequence RXXRXXXGSG (residues 398 to 407) in helix 3 of the M domain. Furthermore, the 2′-OH of A39 is hydrogen-bonded to the phosphate of A63 between the two A-C base pairs of the symmetric loop, directly connecting the two internal loops of the RNA.

Arg-398 and Arg-401 form part of a central salt bridge that includes the invariant Glu-386 and the polypeptide backbone of helix 2b (Fig. 4B). In the structure of the uncomplexed M domain of human SRP54, these side chains were proposed to be inaccessible for direct RNA recognition (*25*). However, with no rearrangement upon RNA binding, these residues form critical contacts to the RNA. Instead of extending into the RNA major or minor grooves, the arginines in the salt bridge present a surface to which the RNA binds. The bridge links the two internal loops of the RNA by way of hydrogen bonds between Arg-401, the N3 of A39 in the asymmetric loop, and the 2′-OH of C62

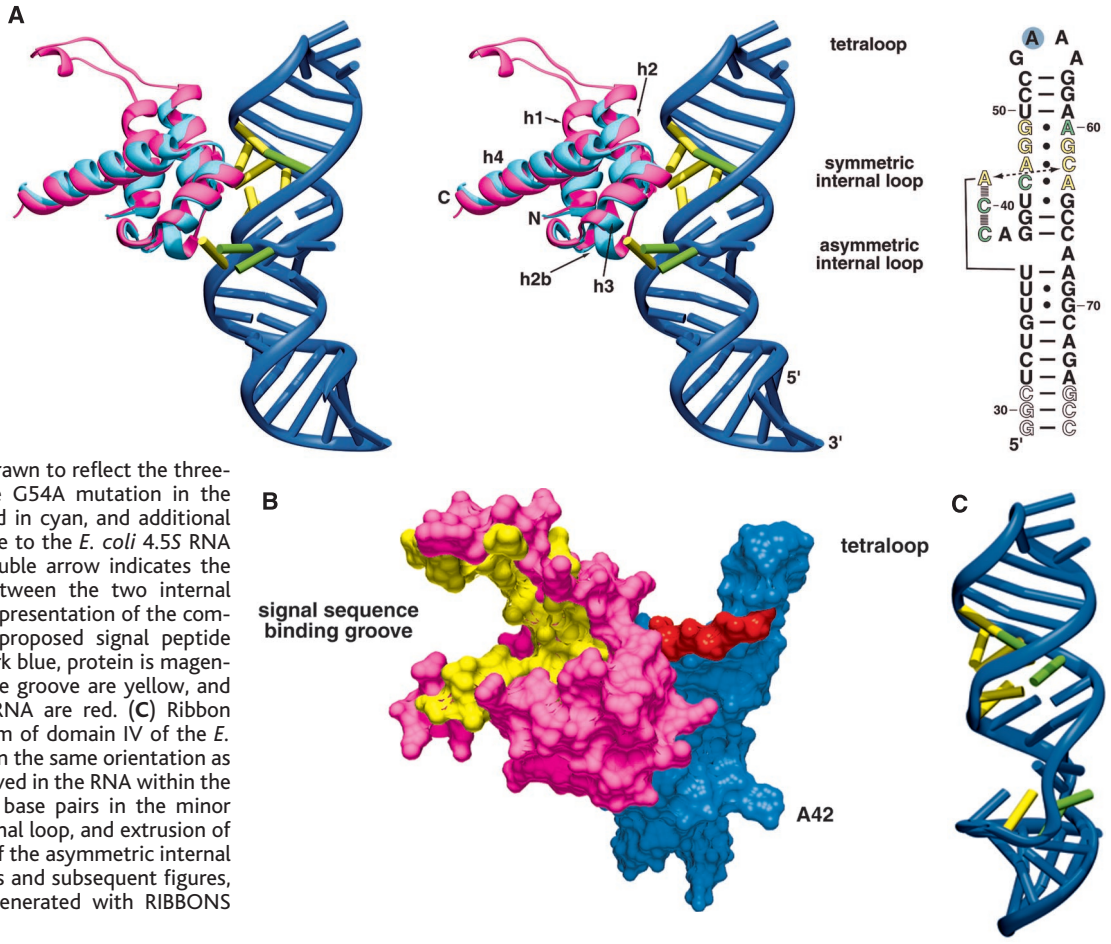

Fig. 2. (**A**) (Left) Stereo representation of the *E. coli* 4.5*S* RNA–M domain structure. The protein is shown as a cyan ribbon; superimposed on the structure is that of the unbound M domain from *T. aquaticus*, drawn as a magenta ribbon. The RNA backbone is represented as a dark blue ribbon, with nucleotides that are universally conserved within SRP RNAs colored yellow and those that are highly conserved colored green. This coloring scheme for the RNA is used in all subsequent figures. (Right) Secondary structure of the RNA used for crystallization drawn to reflect the three-dimensional architecture. The G54A mutation in the crystallized RNA is highlighted in cyan, and additional nucleotides that are not native to the *E. coli* 4.5*S* RNA are shown in outline. The double arrow indicates the tertiary contact observed between the two internal loops. (**B**) Molecular surface representation of the complex, oriented to show the proposed signal peptide recognition groove. RNA is dark blue, protein is magenta; hydrophobic residues in the groove are yellow, and adjacent phosphates in the RNA are red. (**C**) Ribbon representation of the free form of domain IV of the *E. coli* SRP RNA (*16*–*18*), shown in the same orientation as the RNA in (A). Changes observed in the RNA within the complex include exposure of base pairs in the minor groove of the symmetric internal loop, and extrusion of the four bases on the 5′ side of the asymmetric internal loop (see text for details). This and subsequent figures, except where stated, were generated with RIBBONS (*49*).

in the symmetric loop (Fig. 4B). Thus, unlike RNA binding proteins including L11, U1A, U2B″ and sex-lethal (*29*), and L30 (*30*), the M domain of Ffh is preorganized for SRP RNA recognition.

A network of waters and metal ions facilitate the RNA-protein interaction. One of the most striking features of the M domain–RNA complex is the abundance of well-ordered solvent molecules and metal ions that are coordinated to the RNA and, in one case, bridge invariant residues at the RNA-protein interface (Fig. 3A). The extrusion of the asymmetric internal loop nucleotides from the helical stack creates a large cavity in the center of the RNA helix that is filled with cations and water molecules (Fig. 5, A and B). Two hydrated magnesium ions and 28 water molecules were unambiguously identified within this cavity. The waters have temperature factors similar to those of the surrounding atoms of the RNA, indicating that they are highly ordered and occupy specific binding sites (Fig. 5B). In the symmetric loop of the SRP RNA, two potassium ions are coordinated to the noncanonical base pairs. One potassium ion, bound to the carbonyl oxygen of G48 and the N3 and 2′-OH groups of G61 in the G-G base pair, also coordinates to the backbone carbonyl of Gly-405 (Fig. 3A). The functional groups that define this ion-binding pocket are universally conserved in the SRP, suggesting that the potassium ion is integral to their interaction. The other potassium ion is situated between the C46-A63 base pair and the U45-G64 pair in the major groove side of the symmetric internal loop. This ion is also coordinated to several water molecules, forming part of the core of the extensive solvent network in the major groove of the asymmetric loop (Fig. 5, A and B).

To test whether these ions are functionally important for the formation of the SRP complex, we probed their coordination to the RNA using nucleotide analog interference mapping (*31*, *32*). Full-length *E. coli* SRP RNA (110 nt) was transcribed in vitro to contain randomly incorporated 7-deaza adenosine or 2′-deoxyguanosine nucleotide analogs tagged with α-phosphorothioate groups (7dAαS and dGαS, respectively). These analogs were chosen for study because N7 of adenosine and the 2′-OH of guanosine are involved in numerous structural contacts between the RNA and protein. From the resulting pools of RNA, molecules competent to bind to the M domain protein were selected, and positions of incorporated nucleotide analogs were identified by site-specific cleavage.

Six of the RNA functional groups tested in this way were found to make significant energetic contributions to the formation of the SRP complex (Fig. 5C). Strikingly, removal of one of the coordinating ligands to either of the potassium ions seen in the crystal structure

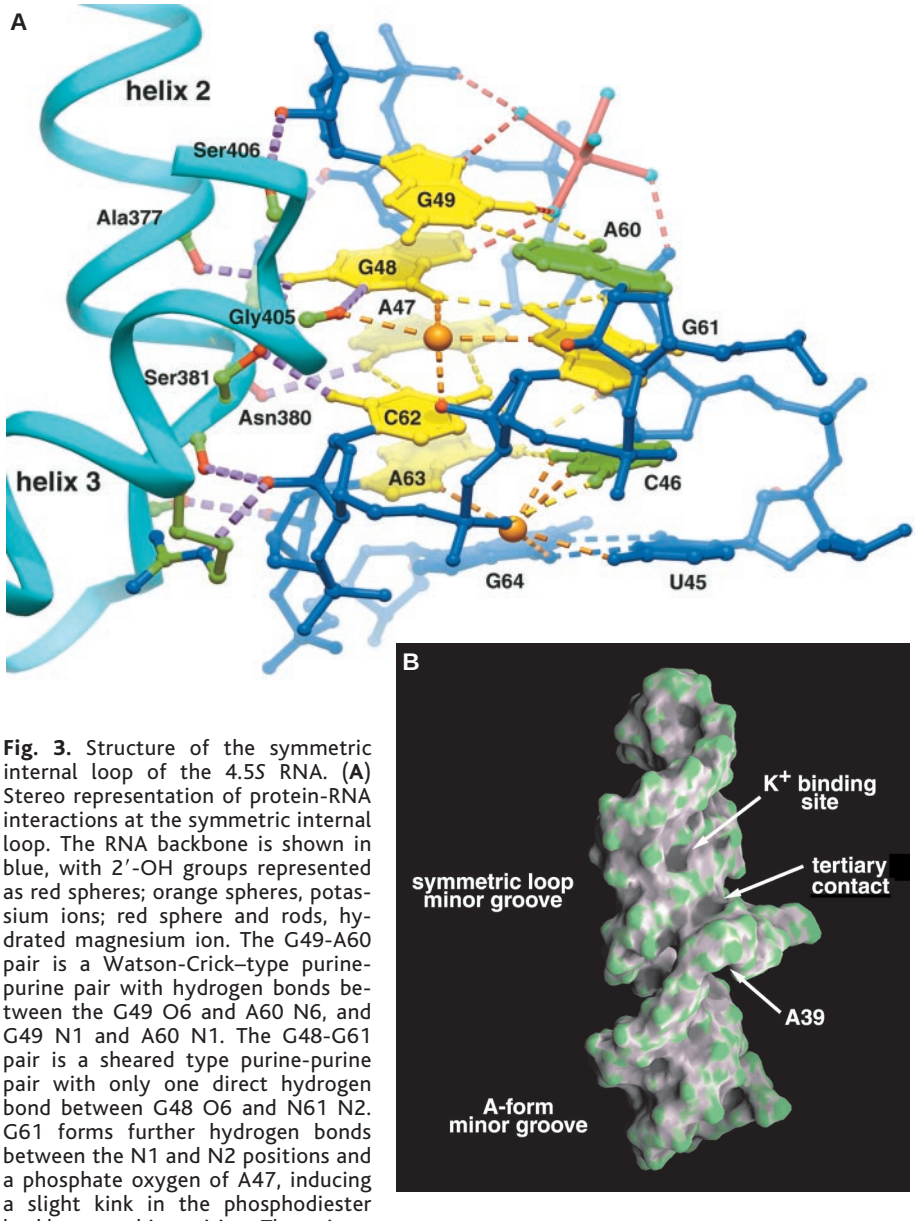

Fig. 3. Structure of the symmetric internal loop of the 4.5*S* RNA. (**A**) Stereo representation of protein-RNA interactions at the symmetric internal loop. The RNA backbone is shown in blue, with 2′-OH groups represented as red spheres; orange spheres, potassium ions; red sphere and rods, hydrated magnesium ion. The G49-A60 pair is a Watson-Crick–type purine-purine pair with hydrogen bonds between the G49 O6 and A60 N6, and G49 N1 and A60 N1. The G48-G61 pair is a sheared type purine-purine pair with only one direct hydrogen bond between G48 O6 and N61 N2. G61 forms further hydrogen bonds between the N1 and N2 positions and a phosphate oxygen of A47, inducing a slight kink in the phosphodiester backbone at this position. The universally conserved A47-C62 form a reverse Hoogsteen pair between A47 N6 and C62 N1, and A47 N7 and C62 N2. The second mismatch contains a single direct hydrogen bond between C46 O2 and A63 N6. This pair has additional base-backbone hydrogen bonds between C46 N4 and a phosphate oxygen of C62, and A63 N6 and C46 O2′. Additionally, the N4 of C62 and O6 of C46 are within hydrogen bonding distance, indicating an additional interaction between these two cytosines to potentially form a "pair of pairs." The extrusion of the reverse-Hoogsteen A47-C62 base pair toward the minor groove presents this pair for recognition by the protein and induces cross-strand stacking between G61 and C46. Ser-381 Oγ forms base-specific hydrogen bonds with the O2 of C62 and N6 of G48. Helix 2 of the M domain makes further base-specific contacts between Ala-377 O and N6 of G48 and Asn-380 and N2 of A47. At the end of helix 3, the conserved GSG sequence participates in RNA recognition through an interaction between Ser-406 O and O2′ of G49 and the coordination of the potassium ion by Gly-405 O. The close approach of the protein backbone to the RNA dictates the requirement of glycine at position 405, whereas Ser-406 and Gly-407 are necessary for maintenance of the turn between helices 3 and 4. All other contacts between the protein and RNA are mediated through hydrogen bonding to 2′-OH groups, while the phosphate oxygens of the symmetric loop are not used by the protein for recognition. (**B**) The molecular surface of the RNA, rotated ~90° around a vertical axis from the view shown in Fig. 2A; coloring is according to the curvature of the surface (green, convex; gray, concave). This representation highlights the relatively flat minor groove of the symmetric internal loop, in which there is a large pocket that binds a potassium ion. The close proximity of the phosphodiester backbones of the two internal loops at the site of a tertiary contact creates a groovelike feature that serves as a site for further RNA-protein interactions. This figure was created with GRASP (*50*).

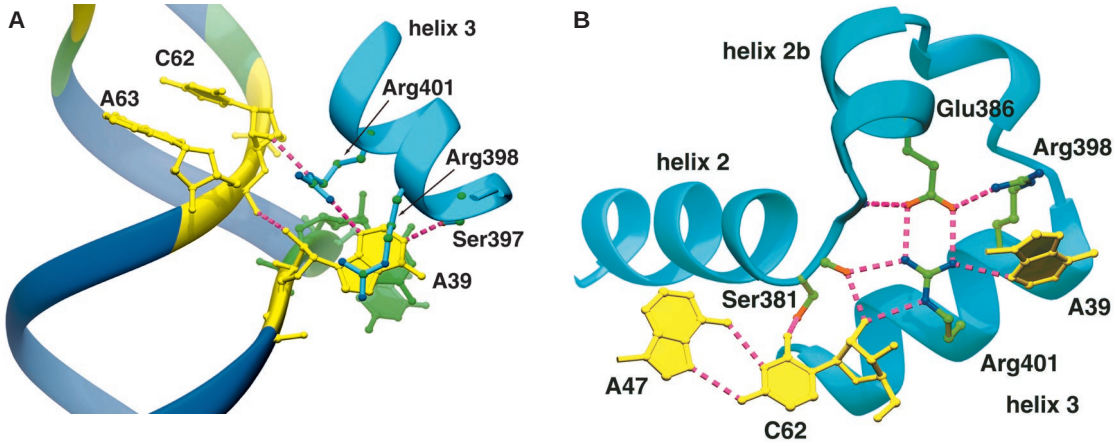

Fig. 4. Asymmetric loop and protein contacts. (**A**) Within the asymmetric loop, nt A39, C40, and C41 form a continuous stack that is capped by Arg-398. Additional contacts are between A39 N3 and NH1 of Arg-401, and A39 N1 and Ser-397 Oγ. Also shown is the single tertiary contact observed in the RNA structure between A39 2′-OH and a phosphate oxygen of A63. (**B**) The heart of the 4.5*S* RNA–M domain interaction consists of a hydrogen bonding network between universally conserved residues. The salt bridge between Glu-386 and Arg-401 is cradled between the asymmetric and symmetric loops of the RNA.

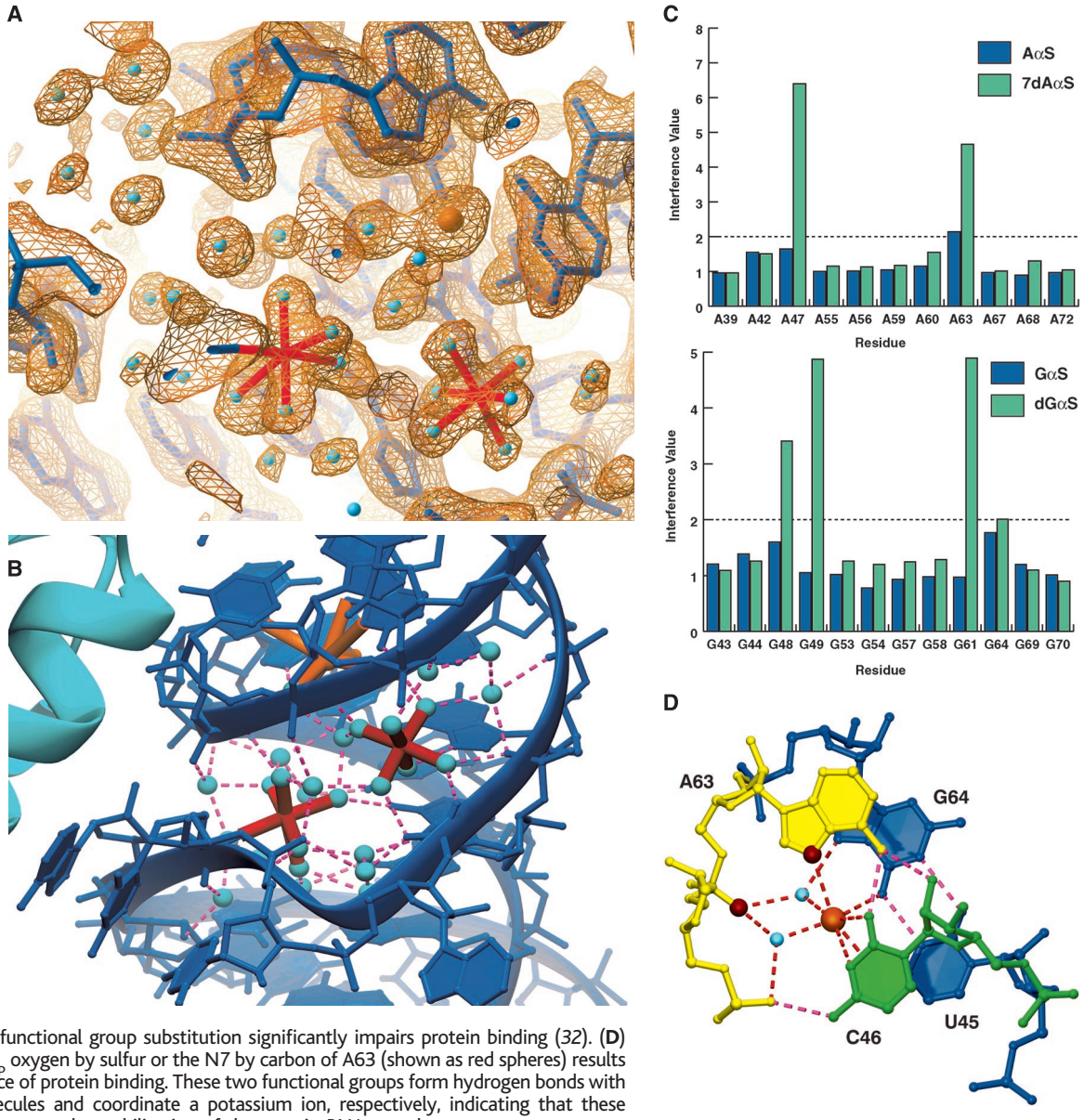

Fig. 5. Metals and solvent in the protein-RNA complex. (**A**) Solvent-flattened experimental electron density map contoured at 1.5 SDs above the mean density level, superimposed on the refined atomic model, shows well-ordered solvent molecules (cyan), hydrated magnesium ions (red), and a potassium ion (orange sphere) located in the interior of the asymmetric internal loop. (**B**) Ribbon and stick diagram of the complex emphasizing the hydrogen bonding network (magenta dashes) between solvent molecules, magnesium ions, and a potassium ion in the asymmetric loop. The average *B* factor for the 28 water molecules represented is 28.5, which is only slightly higher than that of RNA atoms surrounding these solvents, indicating that they are well ordered. (**C**) Histogram of interference values for the M domain binding region of the 4.5*S* RNA; nucleotide positions correspond to the numbering for the *E. coli* 4.5*S* RNA. The dashed line represents an interference value of 2, which is considered to be a site whose functional group substitution significantly impairs protein binding (*32*). (**D**) Substitution of the pro-R_p oxygen by sulfur or the N7 by carbon of A63 (shown as red spheres) results in a significant interference of protein binding. These two functional groups form hydrogen bonds with well-ordered water molecules and coordinate a potassium ion, respectively, indicating that these solvent molecules contribute to the stabilization of the protein-RNA complex.

Table 1. Crystal structure determination and refinement. The 49-nt SRP RNA was transcribed by T7 RNA polymerase and purified by standard techniques (*44*). Selenomethionine-labeled M domain was expressed in the *E. coli* methionine auxotrophic strain B834 (Novagen) and purified with a combination of affinity, reversed-phase, and ion-exchange chromatography. The RNA-protein complex was crystallized by the sitting drop vapor diffusion method by the addition of 2 μl of macromolecular solution to 2 μl of a precipitating solution containing 10% isopropanol, 50 mM Na-MES (pH 5.6), 200 mM KCl, 12.5 mM $MgCl_2$, and 35 mM C-HEGA 10 (Anatrace). Over 2 to 3 days, the crystals grew to maximum cell dimensions of 0.2 mm by 0.1 mm by 0.1 mm, belonging to the *C*2 space group with unit cell dimensions of $a = 136.0$ Å, $b = 77.9$ Å, $c = 32.9$ Å, and $\beta = 96.3°$. For cryoprotection, the crystals were exchanged into mother liquor containing 30% 2,4-methyl pentanediol and flash-frozen in liquid propane. Diffraction data were measured at beamline X4A of the National Synchrotron Light Source and processed with the programs DENZO and SCALEPACK (*45*). Selenium sites were identified and refined with the Crystallography & NMR System (CNS) (*46*), and this phase information plus density modification yielded an electron density map into which most of the RNA and protein could be unambiguously built with the O graphics interface (*47*). Rounds of manual building, torsion-angle simulated annealing, and individual *B*-factor refinement with CNS generated the final model. Magnesium ions were identified by their octahedral coordination geometry as well as the distance (2.1 to 2.2 Å) of inner-sphere coordinated water molecules, whereas potassium ions were identified by their peak height in the electron density (>6.5 SDs above mean density level in each case) as well as inspection of the nature of the functional groups forming inner-sphere coordinations. PROCHECK analysis of the protein revealed that all residues lie within the allowed regions in the Ramachandran plot (92% in the most favorable region) with an overall *G* factor (2.8 bandwidths from the mean) better than that expected for a protein at this resolution (*48*). In the RNA, all sugar puckers are C3′-*endo* except for G58, which is C2′-*exo*, and A42, which was restrained as C2′-*endo* during refinement.

Diffraction data

Wavelength (Å)	Resolution (Å)	Number of reflections observed/unique	Data coverage (%) overall/last shell	$\langle I\rangle/\langle\sigma(I)\rangle$ overall/last shell	R_{sym}* (%) *overall/last shell*
0.9793 (λ_1)	30.0–1.8	141,806/58,274	93.6/72.8	24.6/3.3	3.6/22.1
0.9787 (λ_2)	30.0–1.8	129,140/55,544	88.9/67.2	22.6/2.4	3.7/30.7
0.9667 (λ_3)	30.0–1.8	132,280/56,193	90.1/72.1	21.8/2.2	3.8/32.0

MAD analysis

Phasing power† (acentric reflections)

Resolution range (Å)	λ_1	λ_2	λ_3
30.0–1.8	1.76	2.84	2.62
1.87–1.8	0.89	1.14	0.91

Mean figure of merit‡ (acentric reflections)

Resolution range (Å)	
30.0–1.8	0.68
1.87–1.8	0.37

Refinement

Resolution (Å)	30.0–1.8
Reflections	
Working set	50,840
Test set	5,473 (8.7%)
Total Number of atoms	1,893
Number of waters	299
Number of K^+	3
Number of Mg^{2+}	4
R factor	19.9
R_{free}	22.1
rmsd bond (Å)	0.0065
rmsd angle (°)	1.13
Average *B* factor	31.2

*$R_{sym} = \Sigma|I - \langle I\rangle|/\Sigma I$, where *I* is the observed intensity and $\langle I\rangle$ is the statistically weighted average intensity of multiple measurements of symmetry-related reflections. †Phasing power $= \langle|F_H|\rangle/\langle||F_{PH}| - |F_P + F_H||\rangle$, where $\langle||F_{PH}| - |F_P + F_H||\rangle$ is the residual lack-of-closure error. ‡Mean figure of merit $= \langle\Sigma P(\alpha)e^{i\alpha}/\Sigma P(\alpha)\rangle$, where α is the phase and $P(\alpha)$ is the phase-probability distribution.

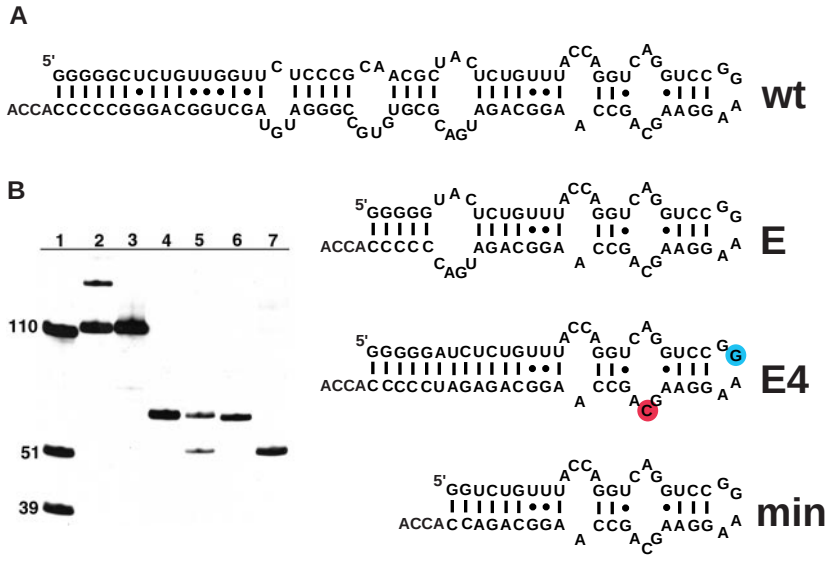

Fig. 6. In vivo function of truncated forms of the SRP RNA. (**A**) Sequences of the RNAs tested for in vivo function. The C62G mutation that was used as a control for proper RNA function is highlighted in red and the G54A tetraloop mutation used in the crystallized RNA is shown in cyan. (**B**) Northern blot analysis of SRP RNAs tested in vivo. *E. coli* S1610 was transformed with plasmids containing wild-type (wt) or minimized (E4 and min) SRP RNAs, followed by a brief heat shock at 45°C to denature the temperature-labile λ repressor and induce genes responsible for prophage excision (*37*). These cultures were allowed to further incubate at 30°C, followed by plating on LB agar. At the permissive temperature (30°C), the chromosomal copy of the 4.5*S* RNA gene is not lost, and thus all cells are viable. At the nonpermissive temperature (42°C), the sole source of SRP RNA is transcribed from a gene encoded on the plasmid. In each case, the RNA with the wild-type domain IV sequence supported cell growth, whereas incorporation of the C62G mutation was lethal (*38*). Total cellular RNA (5 μg) isolated from these transformants wasadded to each lane (2 to 7) alongside RNAs of known length transcribed in vitro (lane 1) and subjected to electrophoresis on a 12% denaturing polyacrylamide gel. The RNA was transferred to a positively charged nylon filter by electroblotting, followed by probing with a psoralen-biotin labeled oligonucleotide that is complementary to nt 32 to 74 of the *E. coli* 4.5*S* RNA; detection was by chemiluminescence. Lane 1, in vitro–transcribed SRP RNAs that are 110, 51, and 39 nt long serve as molecular weight markers; lane 2, RNA from S1610 cells grown at 30°C; lane 3, RNA from cells transformed with a plasmid encoding the wild-type RNA; lane 4, RNA from cells transformed with a plasmid encoding RNA E; lane 5, RNA from cells transformed with a plasmid encoding RNA E4; lane 6, RNA from cells transformed with a plasmid encoding RNA E4 (G54A); lane 7, RNA from cells transformed with a plasmid encoding RNA min. The E4 RNA (lane 5) reproducibly yielded a smaller degradation product, which was also observed in other highly minimized SRP RNAs (*38*).

(dGαS at G61 and 7dAαS at A63) was deleterious to protein binding (Fig. 5, C and D). This result is analogous to observations made in group I self-splicing introns, where potassium ions bind and stabilize RNA tertiary structure (*33*). Furthermore, phosphorothioate substitution alone at A63 interfered with complex formation. Rather than participating in a direct RNA-RNA or RNA-protein contact, this phosphate oxygen is hydrogen-bonded to two well-ordered water molecules that coordinate directly to one of the potassium ions (Fig. 5D). Because these two waters are part of the solvent network seen in the asymmetric loop, this network appears to substantially stabilize the RNA structure required for protein recognition.

Three additional sites where analogs interfere with protein binding are observed in the symmetric internal loop. Two of these involve direct protein-RNA contacts at the 2′-OH groups of G48 and G49 (Fig. 3A). The third, a 7-deaza substitution at A47, disrupts one of the two hydrogen bonds in the A-C base pair at the heart of the RNA-protein interface (Figs. 3A and 4B). Furthermore, results of detailed chemical probing of the 4.5*S* RNA-Ffh interaction (*15*) as well as additional analog interference experiments (*34*) are consistent with the crystal structure. Thus, interactions observed crystallographically are functionally important for formation of the SRP.

In vivo function of the SRP core RNA. Previous studies of the *E. coli* SRP suggested that domain IV of the RNA is necessary and sufficient for specific recognition by Ffh (*15*, *35*) (Fig. 1, B and C). Its binding affinity for the M domain is virtually identical to that for the full-length Ffh protein and it also supports GTP hydrolysis by Ffh and FtsY in vitro (*36*). To test whether the 49-nt domain IV RNA used for crystallography is functional in vivo, we used a strain of *E. coli* (S1610) lysogenic for λ phage carrying the essential gene *ffs* encoding the 4.5*S* RNA (*37*). Under normal growth conditions, the phage is present in the chromosome, the 4.5*S* gene is expressed, and the cells can grow. Upon heat shock the λ lysogen is excised, removing the 4.5*S* gene and preventing bacterial cell growth. This strain is ideal for testing the ability of engineered constructs of the 4.5*S* gene, supplied on plasmids, to support cell growth at the nonpermissive temperature.

Bacterial cells were transformed with plasmids containing a series of constructs of the 4.5*S* RNA gene cloned behind its native promoter (Fig. 6A). When these constructs were expressed from low-copy plasmids, all but the smallest RNA (Fig. 6A, min.) supported growth at the nonpermissive temperature (*38*). The min RNA construct supported growth at the nonpermissive temperature when expressed from a high-copy vector. Analogous RNA constructs containing a point mutation (C62G), which disrupts the protein-RNA interface (Fig. 4B) and thus prevents binding to Ffh (*35*), failed to support growth at the higher temperature (*38*, *39*). As a control for proper RNA expression and processing, and to ensure that endogenous 4.5*S* RNA was absent in cells grown at the nonpermissive temperature, total cellular RNA was tested by Northern blot analysis (Fig. 6B). These results show that all of the SRP RNAs are stable and are correctly processed in vivo. Thus, the nonconserved portion of the SRP RNA is not essential in *E. coli*, though it may play a role in stabilizing the RNA and preventing premature degradation. This demonstrates that the RNA construct that has been crystallized contains all of the elements that are necessary and sufficient for the essential function of the 4.5*S* RNA in vivo.

Although the portion of the SRP RNA outside of the Ffh recognition site is dispensable in vivo, what is the role of the conserved RNA in SRP function? In the crystal structure, the signal peptide binding site proposed by Keenan *et al.* (*24*) lies alongside the RNA backbone adjacent to the symmetric internal loop (Fig. 2, A and B). This creates a continuous molecular surface in which two-thirds of the cleft is contributed by the protein and one-third by the RNA backbone. While signal peptides vary widely in sequence, they are characterized by a hydrophobic region of 6 to 15 amino acids flanked by 2 to 5 positively charged residues. Thus, a binding site composed of both protein and RNA would neatly accommodate such a sequence through a combination of hydrophobic interactions and electrostatic contacts.

The SRP RNA is required to elicit GTP hydrolysis during each cycle of signal sequence binding, protein translocation, and release by the SRP in both bacterial and eukaryotic systems (*40*, *41*). Thus, the RNA–M domain complex (the ribonucleoprotein domain) within the SRP may function analogously to GTPase activating proteins (GAPs) that have been characterized in other GTPase-regulated systems. While most of the universally conserved amino acids and nucleotides are buried in the M domain–RNA interface, A39 and Arg-398 are stacked on the surface of the complex (Fig. 4A). Although invariant within Ffh/SRP54 proteins, Arg-398 is not required for stable association of the SRP RNA with Ffh (*42*), suggesting another role for this region of the SRP core. An intriguing possibility is that the A39–Arg-398 stack modulates GTPase activity of Ffh and/or FtsY (*10*), perhaps by enabling the Arg-398 residue to facilitate GTP hydrolysis as has been observed for other GAPs (*43*).

The structure and analysis of the SRP core presented here provides a detailed understanding of one of the most conserved ribonucleoprotein elements in biology. The unique interactions of protein, RNA, cations, and ordered water molecules create the core of the SRP responsible for signal peptide recognition. Together with earlier crystallographic studies of the NG domain of Ffh (*9*) and the NG domain of the SRP receptor (*11*), structures of the all of the conserved functional centers required for protein translocation by the SRP are now in hand. These structures provide the foundation for understanding how these elements interact to effect protein targeting in all cells.

References and Notes

1. Reviewed in H. Lütcke, *Eur. J. Biochem.* **228**, 531 (1995).
2. Reviewed in P. Walter, *Harvey Lect.* **91**, 115 (1997).
3. G. J. Phillips and T. J. Silhavy, *Nature* **359**, 744 (1992).
4. V. Ribes, K. Romisch, A. Giner, B. Dobberstein, D. Tollervey, *Cell* **63**, 591 (1990).
5. M. A. Poritz *et al.*, *Science* **250**, 1111 (1990).
6. H. D. Bernstein, D. Zopf, D. M. Freymann, P. Walter, *Proc. Natl. Acad. Sci. U.S.A.* **90**, 5229 (1993).
7. J. D. Miller, H. D. Bernstein, P. Walter, *Nature* **367**, 657 (1994).
8. T. Powers and P. Walter, *EMBO J.* **16**, 4880 (1997).
9. D. M. Freymann, R. J. Keenan, R. M. Stroud, P. Walter, *Nature* **385**, 361 (1997).
10. T. Powers and P. Walter, *Science* **269**, 1422 (1995).
11. G. Montoya, C. Svensson, J. Luirink, I. Sinning, *Nature* **385**, 365 (1997).
12. K. Romisch, J. Webb, K. Lingelbach, H. Gausepohl, B. Dobberstein, *J. Cell Biol.* **111**, 1793 (1990).
13. D. Zopf, H. D. Bernstein, A. E. Johnson, P. Walter, *EMBO J.* **9**, 4511 (1990).
14. H. Lutcke, S. High, K. Romisch, A. J. Ashford, B. Dobberstein, *EMBO J.***11**, 1543 (1992).
15. G. Lentzen, H. Moine, C. Ehresmann, B. Ehresmann, W. Wintermeyer, *RNA* **2**, 244 (1996).
16. U. Schmitz *et al.*, *RNA* **2**, 1213 (1996).
17. U. Schmitz, T. L. James, P. Lukavsky, P. Walter, *Nature Struct. Biol.* **6**, 634 (1999).
18. U. Schmitz *et al.*, *RNA* **5**, 1419 (1999).
19. K. Gowda and C. Zwieb, *Nucleic Acids Res.* **25**, 2835 (1997).
20. N. Zheng and L. M. Gierasch, *Mol. Cell* **1**, 79 (1997).
21. T. Samuelsson and C. Zwieb, *Nucleic Acids Res.* **27**, 169 (1999).
22. A fragment of the *E. coli* Ffh corresponding to residues 298 to 453 was probed with V8 and trypsin proteases in the presence and absence of RNA under conditions that yield limited cleavage of the protein. Samples of the proteolytic reaction were taken between 5 min and 1 hour and subjected to matrix-assisted laser desorption/ionization–time-of-flight mass spectrometry [R. C. Beavis and B. T. Chait, *Methods Enzymol.* **270**, 519 (1996)]. Although the free protein was rapidly proteolyzed (<5 min), binding of RNA protected a region corresponding to residues 318 to 432. Further mapping yielded a minimal M domain comprising residues 328 to 432 that still binds to the 4.5*S* RNA with the same affinity as that of full-length Ffh. This construct consists of the signal sequence binding region as well as all of the universally conserved amino acids implicated in RNA recognition (Fig. 1D). Cys-406 was mutated to Ser to avoid oxidation that otherwise destroys RNA binding activity (*24*). In the RNA, the GGAA tetraloop was changed to GAAA to promote RNA-RNA interactions in the crystal lattice.
23. The apparent dissociation constant (K_d) for this RNA-protein interaction was determined with a modification of the nitrocellulose filterbinding assay. Briefly, trace quantities of 5′ end–labeled RNA (<1 pM) were incubated with varying concentrations of M domain in a buffer containing 20 mM K-Hepes (pH 7.5), 100 mM KCl, 10 mM $MgCl_2$, 0.5 mM Na-EDTA, tRNA (0.1 mg/ml), and 0.01% Igepal C-630 for 30 min at room temperature. These reaction mixtures were then filtered through a nitrocellulose filter (BA85, Schleicher & Schuell) and a positively charged nylon filter (Hybond+, Amersham). The filters were washed with two 200-μl samples of binding buffer, and the radioactivity corresponding to free and bound quantified with a PhosphorImager (Molecular Dynamics). The fraction of RNA bound was fit to a Langmuir isotherm to yield K_d.

24. R. J. Keenan, D. M. Freymann, P. Walter, R. M. Stroud, *Cell* **94**, 181 (1998).
25. W. M. Clemons Jr., K. Gowda, S. D. Black, C. Zwieb, V. Ramakrishnan, *J. Mol. Biol.* **292**, 697 (1999).
26. The least-squares superposition of backbone α carbons corresponding to the RNA binding region of the bound M domain (*E. coli* residues 376 to 421), *Thermus aquaticus* [Protein Data Bank (PDB) accession number 2ffh], and human M domain (1QB2) were performed with LSQMAN [G. J. Kleywegt and T. A. Jones, *CCP4 Newslett.* **31**, 9 (1994)]. The backbone root mean square deviation (rmsd) between the *E. coli* and *T. aquaticus* M domains is 0.68 Å, and 0.66 Å between the *E. coli* and human M domains.
27. R. Wintjens and M. Rooman, *J. Mol. Biol.* **262**, 294 (1996).
28. B. Luisi, in *DNA-Protein: Structural Interactions*, D. M. J. Lilley, Ed. (Oxford Univ. Press, Oxford, 1995), pp. 1–49.
29. Reviewed in D. E. Draper, *J. Mol. Biol.* **293**, 255 (1999).
30. H. Mao, S. A. White, J. R. Williamson, *Nature Struct. Biol.* **6**, 1139 (1999).
31. S. A. Strobel, *Biopolymers* **48**, 65 (1998).
32. Nucleotide analog interference mapping was performed as described [S. P. Ryder and S. A. Strobel, *Methods* **18**, 38 (1999)]. In brief, phosphorothioate-tagged nucleotide analogs were incorporated randomly into the 4.5*S* RNA at the 5% level by run-off transcription by T7 RNA polymerase. This RNA was 5′ ^{32}P end-labeled and incubated with M domain at a concentration of 25 pM under standard binding conditions (*23*). This reaction was passed through a nitrocellulose filter to select for protein-bound RNA, the retained RNA eluted off the filter, and ethanol precipitated. The RNA pellet was resuspended in 10 μl of doubly distilled H_2O and 10 μl of formamide load buffer, and in parallel with control unselected RNA, the phosphorothioate linkages were cleaved by the addition of 1 μl of 1 mM I_2-ethanol solution and incubation at 90°C for 1 min. The cleavage products were resolved by electrophoresis on a 12% denaturing polyacrylamide gel. The band intensities were quantified by phosphorimaging and the extent of interference determined as described [S. P. Ryder and S. A. Strobel, *Methods* **18**, 38 (1999)].
33. S. Basu *et al.*, *Nature Struct. Biol.* **5**, 986 (1998).
34. A number of other nucleotide analogs, including 2′ deoxyadenosine, diamino purine, inosine, and *N*-methyl guanosine, have also been used, and the results are consistent with the crystal structure.
35. H. Wood, J. Luirink, D. Tollervey, *Nucleic Acids Res.* **20**, 5919 (1992).
36. R. T. Batey, L. Lucast, J. A. Doudna, unpublished data.
37. S. Brown, G. Thon, E. Tolentino, *J. Bacteriol.* **171**, 6517 (1989).
38. R. T. Batey, B. Rha, J. A. Doudna, data not shown.
39. The A39U point mutation in the context of the E4 construct was also tested and failed to support growth.
40. J. D. Miller, H. Wilhelm, L. Gierasch, R. Gilmore, P. Walter, *Nature* **366**, 351 (1993).
41. J. D. Miller, S. Tajima, L. Lauffer, P. Walter, *J. Cell Biol.* **128**, 273 (1995).
42. K. Kurita *et al.*, *J. Biol. Chem.* **271**, 13140 (1996).
43. S. J. Gamblin and S. J. Smerdon, *Curr. Opin. Struct. Biol.* **8**, 195 (1998).
44. J. A. Doudna, *Methods Mol. Biol.* **74**, 365 (1997).
45. Z. Otwinoski and W. Minor, *Methods Enzymol.* **276**, 307 (1997).
46. A. T. Brunger *et al.*, *Acta Crystallogr. D* **54**, 905 (1998).
47. T. A. Jones, J. Y. Zou, S. W. Cowan, Kjeldgaard, *Acta Crystallogr. A* **47**, 110 (1991).
48. R. J. Laskowski, M. W. Macarthur, D. S. Moss, J. M. Thornton, *J. Appl. Crystallogr.* **26**, 283 (1993).
49. M. Carson, *J. Appl. Crystallogr.* **24**, 958 (1991).
50. A. Nicholls, K. A. Sharp, B. Honig, *Proteins* **11**, 281 (1991).
51. We thank S. Brown for providing the 4.5*S* RNA conditionally deficient strains of *E. coli* and helpful advice; C. Ogata for time and assistance at beamline X4A of the National Synchrotron Light Source, Brookhaven National Laboratory; T. Earnest for support at beamline 5.0.2 of the Advanced Light Source, Lawrence Berkeley National Laboratory; R. Hanna, J. Kieft, A. Luptak, and M. Talavera for help with beamline data collection and useful discussions; P. Adams and L. Rice for assistance with the refinement; the staff of the Yale Center for Structural Biology for crystallographic and computational support; S. Strobel for providing the nucleotide analogs and for helpful discussions; S. Basu, J. Cate, J. Davis, T. Griffin, J. Ippolito, S. Ryder, P. Scamborova, P. Sigler, and T. Steitz for many helpful discussions; and J. Cate, J. Kieft, V. Rath, and S. Strobel for critically reading the manuscript. We are particularly indebted to A. Ferré-D'Amaré for excellent advice and support throughout this project. This project was funded in part by a postdoctoral fellowship from the Jane Coffin Childs Memorial Fund for Medical Research (R.T.B.), a Howard Hughes Medical Institute (HHMI) summer fellowship (B.R.), and by support from the NIH, HHMI, and the David and Lucile Packard Foundation. J.A.D. is a Fellow of the David and Lucile Packard Foundation and an Assistant Investigator of HHMI. Coordinates of the SRP core and structure factor amplitudes have been deposited in the PDB (accession code 1DUL). Coordinates are also available at www.csb.yale.edu/people/doudna/doudna_people.html.

14 December 1999; accepted 12 January 2000

Three-Layered Atmospheric Structure in Accretion Disks Around Stellar-Mass Black Holes

S. N. Zhang,[1,2]* Wei Cui,[3] Wan Chen,[4,5] Yangsen Yao,[1] Xiaoling Zhang,[1] Xuejun Sun,[1] Xue-Bing Wu,[6] Haiguang Xu[7]

Modeling of the x-ray spectra of the Galactic superluminal jet sources GRS 1915+105 and GRO J1655-40 reveals a three-layered atmospheric structure in the inner region of their accretion disks. Above the cold and optically thick disk with a temperature of 0.2 to 0.5 kiloelectron volts, there is a warm layer with a temperature of 1.0 to 1.5 kiloelectron volts and an optical depth around 10. Sometimes there is also a much hotter, optically thin corona above the warm layer, with a temperature of 100 kiloelectron volts or higher and an optical depth around unity. The structural similarity between the accretion disks and the solar atmosphere suggests that similar physical processes may be operating in these different systems.

The sun has a complicated atmosphere, including a photosphere, a chromosphere, a transition layer, and an outermost hot corona (*1*, *2*). It is generally thought that the magnetic activities of the sun may play an important role in heating the corona (*2*, *3*), although other models have been proposed (*4*). The atmosphere of the sun is not in hydrodynamical equilibrium. Consequently, the solar wind is blown outward from the corona. Coronas and outflows are actually common in various types of stellar environments. Here, we present observational evidence and modeling for a solar-type atmosphere for the accretion disks around stellar-mass black holes in x-ray binaries (*5*).

One of the common characteristics of black hole binaries is the so-called two-component x-ray and gamma-ray spectrum: a soft blackbody-like component at low energies (<10 keV) and a hard power-law–like component at high energies (up to several hundred keV) (*6*). The soft component is generally attributed to the emission from an optically thick, geometrically thin cold accretion disk, which is often described by the standard α-disk model (*7*). The hard component is attributed to an optically thin, geometrically thick hot corona in either a plane parallel to the disk or with a spherical geometry above the disk (*8*). The prototype models were motivated by the studies of the solar corona (*9*).

Recently, more attention has been paid to

[1]Physics Department, University of Alabama in Huntsville, Huntsville, AL 35899, USA. [2]Space Sciences Laboratory, NASA Marshall Space Flight Center, SD50, Huntsville, AL 35812, USA. [3]Center for Space Research, Massachusetts Institute of Technology, Cambridge, MA 02139, USA. [4]Department of Astronomy, University of Maryland, College Park, MD 20742, USA. [5]NASA/Goddard Space Flight Center, Code 661, Greenbelt, MD 20771, USA. [6]Beijing Astronomical Observatory, Chinese Academy of Sciences, Beijing 100012, People's Republic of China. [7]Institute for Space and Astrophysics, Department of Applied Physics, Shanghai Jiao-Tong University, Shanghai 200030, People's Republic of China.

*To whom correspondence should be addressed. E-mail: zhangsn@email.uah.edu